Solid State Nuclear Magnetic Resonance 80 (2016) 7–13

Contents lists available at ScienceDirect

Solid State Nuclear Magnetic Resonance

journal homepage: www.elsevier.com/locate/ssnmr

Calculation of solid-state NMR lineshapes using contour analysis

Colan E. Hughes*, Kenneth D.M. Harris*

School of Chemistry, Cardiff University, Park Place, Cardiff, Wales CF10 3AT, UK

A B S T R A C T

Two new methods for calculating lineshapes in solid-state NMR spectra are described. The first method, which we refer to as semi-analytical, allows the rapid calculation of quadrupolar central-transition lineshapes in both static and magic-angle spinning cases. The second method, which is fully numerical, allows the calculation of lineshapes resulting from any combination of interactions, including quadrupolar, dipolar and chemical shift anisotropy, and is not restricted to cases in which the principal axis systems for the different interactions are aligned. Both methods are derived from consideration of the contour lines on a plot of the resonance frequency against the Euler angles, allowing the intensity of the lineshape to be calculated at each frequency. Consequently, highly accurate lineshapes can be calculated more rapidly than previously possible, since only orientations contributing to each specific frequency are considered. For our semi-analytical method, the intensity of each point in the lineshape can be directly calculated in tens of milliseconds on a standard PC. In contrast, established methods can take several hours to calculate the same lineshape.

1. Introduction

The calculation of lineshape functions for NMR spectra can be traced back to the work of Pake [1] in 1948 and Bloembergen and Rowland [2] in 1953. In the paper by Pake, the lineshape function for a pair of dipolar-coupled protons was calculated, consisting of two parts which form the famous “Pake doublet”. Bloembergen and Rowland used the same methodology as Pake to derive the lineshape function for a non-axial Knight shift in metals. This interaction has the same angular dependence as first-order quadrupolar coupling and chemical shift anisotropy, to which it is directly analogous. Consequently, the function of Bloembergen and Rowland can be used wherever a single interaction of these types dominates the lineshape.

For quadrupolar nuclei [3], the different transitions have different dependences upon the quadrupolar interaction. In particular, for half-integer spins, the central transition is not broadened to first order whereas, for integer spins, all the transitions are affected. Consequently, the function of Bloembergen and Rowland can be used for the satellite transitions of half-integer spin quadrupolar nuclei and for all the transitions of integer-spin nuclei such as ^{2}H. However, as is well established [4], the quadrupolar coupling is often sufficiently large with respect to the Zeeman interaction that a first-order analysis does not fully describe the lineshapes. In such cases, second-order effects must be taken into account.

Using perturbation theory, the second-order dependence of the resonance frequency on the quadrupolar interaction can be determined under both static [4] and magic-angle spinning (MAS) [5] conditions. In both cases, the central transition for half-integer quadrupolar nuclei *is* broadened, leading to many spectroscopic challenges which have created one of the most fertile grounds for experimental developments in the field of solid-state NMR (for example, leading to DOR [6], DAS [7], MQMAS [8] and STMAS [9]). With many experiments designed to extract isotropic spectra of quadrupolar nuclei, there is, nevertheless, continuing interest in the lineshapes of the second-order quadrupolar central transition for half-integer spin nuclei [10,11], particularly with a view to extracting structural information from values of the quadrupolar coupling constant and asymmetry parameter.

If the methodology of Pake, Bloembergen and Rowland is followed to derive formulae for more mathematically complicated interactions, a point is reached at which the derivation cannot continue. This failure has led to the widespread use of an alternative method for calculating lineshapes for such interactions, whereby the resonance frequencies for a large number of crystallite orientations (expressed as pairs of Euler angles) are calculated and used to build up the lineshape [12]. To be efficient, this methodology requires a set of Euler angle pairs to be chosen which are evenly distributed over the surface of a sphere, particularly in regions where the function for the resonance frequency passes through turning points. As a consequence, several methods have been devised to calculate suitable angle sets [13], including ZCW [14–16], ASG [17], SOPHE [18], REPULSION [19], LEB [20], SHREWD [20] and SPIRAL [21]. Whilst the symmetry of the resonance frequency with respect to the Euler

* Corresponding authors.
E-mail addresses: HughesCE@cardiff.ac.uk (C.E. Hughes), HarrisKDM@cardiff.ac.uk (K.D.M. Harris).

http://dx.doi.org/10.1016/j.ssnmr.2016.10.002
Received 15 August 2016; Received in revised form 22 September 2016; Accepted 5 October 2016
Available online 13 October 2016

angles can allow simulation across only portions of the sphere to be used [20], these angle sets are typically required to be very large in order to obtain the required even distribution.

In two recent papers, Field and Bain examined the second-order quadrupolar central-transition lineshapes under static [10] and MAS [11] conditions, focusing on the singularities in these lineshapes as a means of identifying the values of the quadrupole coupling constant and asymmetry parameter without recourse to full simulation of the lineshape. To demonstrate their method, lineshape functions were calculated across the full range of asymmetry parameters. For each of these calculations, nearly 3.3×10^{10} pairs of Euler angles were used, taking *ca.* 15 h on a standard personal computer, thus clearly demonstrating the advantage of their method of considering the singularities rather than the full lineshape, given the required simulation time.

In this paper, we propose a different approach and consider why the method of Pake, Bloembergen and Rowland fails. As discussed below, for the case of the second-order quadrupolar central-transition lineshapes, it is the final integration step which proves impossible (except for axial symmetry). We therefore replace analytical integration by numerical integration, leading to a method that is far faster than those employing large sets of Euler angle pairs. We then consider more complicated cases, where the first step of the method of Pake, Bloembergen and Rowland proves intractable. Here, we recognize that their method can be carried out wholly numerically by identifying the sets of Euler angle pairs which correspond to the contour lines for each value of the resonance frequency on a plot of resonance frequency *versus* Euler angles. Although slower than our first method, by only considering Euler angle pairs giving rise to each specific frequency in the lineshape, this method still has the potential to be much more efficient than previous methods.

An earlier attempt to calculate analytical forms for the lineshapes of quadrupolar nuclei was made by Ajoy et al. [22] Their method breaks up the lineshape into distinct regions between the steps and singularities. Unfortunately, their results are expressed in very lengthy formulae, at least some of which still require numerical integration to generate the lineshape. Perhaps as a consequence, this method has not been adopted in the analysis of quadrupolar lineshapes.

2. The analytical method

We first review the analytical method for obtaining lineshape functions. For a generic orientationally dependent interaction, the resonance frequency for a given crystallite orientation, defined by the Euler angles α and β, can be expressed as

$$\omega = \omega_0\delta_{iso} + A\,f(\alpha, \beta), \tag{1}$$

where the dimensionless function $f(\alpha, \beta)$ determines the lineshape, the term A scales this shape in the frequency dimension and $\omega_0\delta_{iso}$ determines the isotropic frequency of the lineshape. The resulting powder pattern, assuming an isotropic distribution of crystallite orientations, can be derived by considering two probability distributions: (i) $P(f)$ is the probability of a crystallite having resonance frequency f and is proportional to the intensity of the lineshape at f, and (ii) $P(\alpha, \beta)$ is the probability of a crystallite having the orientation defined by Euler angles α and β, and is given by $1/(4\pi)\sin(\beta)$. Integrating $P(f)$ over f and integrating $P(\alpha, \beta)$ over α and β must give the same result, corresponding to the whole sample. Hence

$$\int_{f_{\min}}^{f_{\max}} P(f)\,df = \int_0^{2\pi}\int_0^{\pi} P(\alpha, \beta)\,d\beta\,d\alpha. \tag{2}$$

Defining $P(f, \alpha)$ as the powder pattern corresponding to a specific value of α, we can write

$$P(f) = \int_0^{2\pi} P(f, \alpha)\,d\alpha, \tag{3}$$

and therefore

$$\int_0^{2\pi}\int_{f_{\min}}^{f_{\max}} P(f, \alpha)\,df\,d\alpha = \frac{1}{4\pi}\int_0^{2\pi}\int_0^{\pi} \sin(\beta)\,d\beta\,d\alpha. \tag{4}$$

The integrations not over α may be extracted, resulting in

$$\int_{f_{\min}}^{f_{\max}} P(f, \alpha)\,df = \frac{1}{4\pi}\int_0^{\pi} \sin(\beta)\,d\beta, \tag{5}$$

which can be rearranged to give

$$P(f, \alpha) = \frac{\mu}{4\pi}\sin(\beta(f, \alpha))\left|\frac{\partial\beta(f, \alpha)}{\partial f}\right|, \tag{6}$$

where the term $\beta(f, \alpha)$ expresses the Euler angle β as a function of f and α. The term μ is a multiplicity term, which is necessary as the function for f generally repeats over the range of values of β. The term $P(f, \alpha)$ may be inserted into Eq. (3) to give the following expression for the lineshape:

$$P(f) = \int_0^{2\pi} \frac{\mu}{4\pi}\sin(\beta(f, \alpha))\left|\frac{\partial\beta(f, \alpha)}{\partial f}\right| d\alpha. \tag{7}$$

The integration is most readily performed over $\cos(2\alpha)$ between −1 and +1. Introducing this change of variable gives

$$P(f) = \int_{-1}^{1} \frac{\mu}{2\pi}\frac{\sin(\beta(f, \alpha))}{\sqrt{1-\cos^2(2\alpha)}}\left|\frac{\partial\beta(f, \alpha)}{\partial f}\right| d(\cos(2\alpha)). \tag{8}$$

For the first-order quadrupolar case, this substitution allows an analytical solution to be derived [2]. Substitution for f using

$$f = \frac{\omega - \omega_0\delta_{iso}}{A}, \tag{9}$$

and applying an appropriate vertical scaling allows the final lineshape to be determined.

Thus, to obtain a lineshape function requires three steps.

1. The equation for the resonance frequency must be solved to find a function for the Euler angle β in terms of the resonance frequency, f, and the other Euler angle, α.
2. This function must be differentiated with respect to the resonance frequency and the sine of the function must be determined.
3. These two terms are then inserted into Eq. (8) and integration is carried out with respect to $\cos(2\alpha)$.

This simple derivation hides two important points. First, in order to determine β as a function of f and α, multiple solutions may arise. In some cases, the different solutions may give identical contributions to the lineshape and can be absorbed into the multiplicity term μ. However, in other cases, the different solutions may be quite distinct and therefore necessitate separate integrations to be added together to obtain the final lineshape.

The second important point concerns limits. The turning points of the function $f(\alpha, \beta)$ can be identified by differentiating with respect to α and β. Inspection of the function(s) $\beta(f, \alpha)$ indicates which of these turning points represents the limiting values of f for each contribution. In addition, the limits for integration over α must also be considered, recognizing that only those values of α for which the integrand is real need to be considered. Depending on the method used for the integration, this may require explicit definition of the integration limits within a number of distinct ranges of f.

Plotting $\beta(f, \alpha)$ for a fixed value of f as a function of α demonstrates that these functions correspond to the lines on a contour plot of f against α and β. This point is not of significance with regard to our semi-analytical method detailed below but it is at the heart of our fully-numerical method described later.

2.1. Second-order quadrupolar central-transition lineshapes

We now attempt to apply this analytical method to the case of second-order broadening of the central transition for a half-integer quadrupolar nucleus under static and MAS conditions. The resonance frequency for the central transition under both static and MAS conditions can be expressed as

$$\omega_{CT} = \omega_0\delta_{iso} + A_Q f_Q, \tag{10}$$

where

$$\begin{aligned} A_Q &= \frac{(2I+3)\chi^2}{256I^2(2I-1)\omega_0}, \\ f_Q^{(Static)} &= \sum_{m=0}^{2}\sum_{n=0}^{2}\kappa_{m,n}^{(Static)}\cos^n(2\alpha_{PL})\cos^{2m}(\beta_{PL}), \\ f_Q^{(MAS)} &= \sum_{m=0}^{2}\sum_{n=0}^{2}\kappa_{m,n}^{(MAS)}\cos^n(2\alpha_{PR})\cos^{2m}(\beta_{PR}). \end{aligned} \tag{11}$$

Here, I is the nuclear spin, χ is the quadrupolar coupling constant (given by $e^2qQ/\hbar$), η is the asymmetry parameter, PL indicates that the Euler angles in the static case relate the principal axis system (PAS) of the quadrupolar interaction to the laboratory frame and PR indicates that the Euler angles in the MAS case relate the PAS of the quadrupolar interaction to the rotor frame. The terms $\kappa_{m,n}^{(Static)}$ are given by [4]

$$\begin{aligned} &\kappa_{0,0}^{(Static)} = 9 - 8\eta^2,\ \kappa_{0,1}^{(Static)} = -6\eta,\ \kappa_{0,2}^{(Static)} = 9\eta^2, \\ &\kappa_{1,0}^{(Static)} = 6(2\eta^2 - 15),\ \kappa_{1,1}^{(Static)} = -48\eta,\ \kappa_{1,2}^{(Static)} = -18\eta^2, \\ &\kappa_{2,0}^{(Static)} = 81,\ \kappa_{2,1}^{(Static)} = 54\eta,\ \kappa_{2,2}^{(Static)} = 9\eta^2. \end{aligned} \tag{12}$$

and the terms $\kappa_{m,n}^{(MAS)}$ are given by [5]

$$\begin{aligned} &\kappa_{0,0}^{(MAS)} = -\tfrac{15}{2},\ \kappa_{0,1}^{(MAS)} = -3\eta,\ \kappa_{0,2}^{(MAS)} = -\tfrac{7}{2}\eta^2, \\ &\kappa_{1,0}^{(MAS)} = 27 - 2\eta^2,\ \kappa_{1,1}^{(MAS)} = 24\eta,\ \kappa_{1,2}^{(MAS)} = 7\eta^2, \\ &\kappa_{2,0}^{(MAS)} = -\tfrac{63}{2},\ \kappa_{2,1}^{(MAS)} = -21\eta,\ \kappa_{2,2}^{(MAS)} = -\tfrac{7}{2}\eta^2. \end{aligned} \tag{13}$$

Although the Euler angles relate to different reference frames in the static and MAS cases, we note that this distinction does not make any difference to the following discussion, as both pairs of Euler angles are distributed over the same range with the same probabilities. For the general discussion, we henceforth refer simply to α and β. Note also that we have used the convention [23] $|V_{zz}| \geq |V_{xx}| \geq |V_{yy}|$ with $\eta = (V_{yy} - V_{xx})/V_{zz}$ for the electric field gradient tensor. The alternative convention [24] ($|V_{zz}| \geq |V_{yy}| \geq |V_{xx}|$ with $\eta = (V_{xx} - V_{yy})/V_{zz}$) differs only by a 90° shift in the values of the Euler angles α_{PL} and α_{PR}.

Given that Eq. (10) applies to both the static and MAS cases, we can proceed to derive general equations and later insert the specific values for A_Q and $\kappa_{m,n}$. To find β in terms of f_Q, we start with

$$f_Q = a + b\cos^2(\beta) + c\cos^4(\beta), \tag{14}$$

where a, b and c are functions of $\cos(2\alpha)$ and $\kappa_{m,n}$. There are two solutions to this quadratic equation in $\cos^2(\beta)$

$$\beta_{\pm}(f_Q, \alpha) = \cos^{-1}\left(\sqrt{\frac{-b \pm \sqrt{b^2 + 4c(f_Q - a)}}{2c}}\right). \tag{15}$$

Plotting these functions for any values of f, α and η shows that together they cover the range $0 \leq \beta \leq \frac{1}{2}\pi$ but do not represent the same shape and must be treated separately, each with a multiplicity μ_i=2, in order to cover the range $0 \leq \beta \leq \pi$. If we define $\xi = \sqrt{b^2 + 4c(f_Q - a)}$, the derivatives with respect to f are given by

$$\left|\frac{\partial\beta_{\pm}(f_Q, \alpha)}{\partial f_Q}\right| = \frac{c}{\xi\sqrt{(b + 2c \mp \xi)(-b \pm \xi)}}, \tag{16}$$

and the sine terms are

$$\sin(\beta_{\pm}(f_Q, \alpha)) = \sqrt{\frac{b + 2c \mp \xi}{2c}}, \tag{17}$$

Hence, the integrands defined by Eq. (6) are given by

$$P_{\pm}(f_Q, \alpha) = \frac{\sqrt{c}}{2\sqrt{2}\,\pi\,\xi\sqrt{-b \pm \xi}}. \tag{18}$$

Each of these terms must be integrated over α to give the separate contributions to the lineshape.

Changing variables to cos(2α) allows the two distinct integrands to be expressed as

$$\begin{aligned} P_1(f_Q,\ \cos(2\alpha)) &= \frac{\sqrt{c}}{\sqrt{2}\pi\sqrt{1-\cos^2(2\alpha)}\ \xi\sqrt{-b+\xi}}, \\ P_2(f_Q,\ \cos(2\alpha)) &= \frac{\sqrt{c}}{\sqrt{2}\pi\sqrt{1-\cos^2(2\alpha)}\ \xi\sqrt{-b-\xi}}, \end{aligned} \tag{19}$$

with the terms b, c and ξ defined for the static case as

$$\begin{aligned} b^{(Static)} &= 6(-15 + \eta(2\eta - (8 + 3\eta\cos(2\alpha_{PL}))\cos(2\alpha_{PL}))), \\ c^{(Static)} &= 9(3 + \eta\cos(2\alpha_{PL}))^2, \\ \xi^{(Static)} &= 6\sqrt{4(6 + 5\eta\cos(2\alpha_{PL}) + \eta^2)^2 + (3 + \eta\cos(2\alpha_{PL}))^2(f_Q^{(Static)} - 4\eta^2)}. \end{aligned} \tag{20}$$

and for the MAS case as

$$\begin{aligned} b^{(MAS)} &= -27 + \eta(2\eta - (24 + 7\eta\cos(2\alpha_{PR}))\cos(2\alpha_{PR})), \\ c^{(MAS)} &= \tfrac{7}{2}(3 + \eta\cos(2\alpha_{PR}))^2, \\ \xi^{(MAS)} &= \sqrt{2} \\ &\quad \sqrt{2(18 + 9\eta\cos(2\alpha_{PR}) + \eta^2)^2 - 7(3 + \eta\cos(2\alpha_{PR}))^2(f_Q^{(MAS)} + 2(6 + \eta^2))}. \end{aligned} \tag{21}$$

For the case of axial symmetry, for which η=0, the integrands are far simpler and can be easily integrated, since the integrands (and, indeed, the interactions themselves) are independent of α. The solutions [25,26] are set out in Supplementary Information.

Unfortunately, when $\eta \neq 0$, we have found that integration by analytical solution is intractable. Consequently, we must use numerical integration at this final step. For each value of f_Q, we need to integrate the two integrands over the appropriate range of values of $\cos(2\alpha)$ (where they are real) to obtain the intensity at that value of f_Q. Although accurate numerical integration requires identification of the limiting values for each integration (as set out below), this method is far faster than the conventional method and can be easily tailored, by selecting the step size in f_Q, to give the desired spectral resolution. We call this method "semi-analytical", since it requires analytical forms to be derived before numerical integration is applied.

3. The "semi-analytical" method

All the functions that we are integrating contain singularities as the terms $P_i(f_Q,\ \cos(2\alpha))^{-1}$ are equal to zero for certain values of f_Q and $\cos(2\alpha)$. In order for numerical integration to give an accurate result, it must be performed between limiting values that correspond to these singularities, so that the software may recognize and treat the singularities appropriately. We therefore need to either define the singularities analytically or use a procedure which pinpoints the singularities before carrying out numerical integration. Following the work of Field and Bain [10,11], which identified all the turning points in the functions for both static and MAS cases, we take the first approach.

The stationary points of the functions $f_Q^{(Static)}$ and $f_Q^{(MAS)}$ can be determined by simple calculus and correspond to the steps (for the maxima and minima) and singularities (for the saddle points) in the lineshapes [4,5]. For both the static [10] and MAS [11] cases (see Table S1 in Supplementary Information), inserting the maxima and minima into the two solutions (Eq. (19)) for β determines the range of values over which the solutions are real and can contribute to the lineshape. For the static case, the first solution is real over the range

$$-16(\eta+1)<f_Q^{(Static)}<4\eta^2, \tag{22}$$

and the second solution is real over the range

$$-16(\eta+1)<f_Q^{(Static)}<(3+\eta)^2. \tag{23}$$

For the MAS case, the first solution is real over the range

$$-2(6+\eta^2)<f_Q^{(MAS)}<-\frac{12}{7}(1-\eta)^2, \tag{24}$$

and the second solution is real over the range

$$-\frac{7}{2}\eta^2-3\eta-\frac{15}{2}<f_Q^{(MAS)}<-\frac{12}{7}(1-\eta)^2. \tag{25}$$

Within these ranges for f_Q, the values of $\cos(2\alpha)$ between which the integrands are real depends upon the value of f_Q. The analytical forms of these limits can be found by solving the equation $P_i(f_Q,\ \cos(2\alpha))^{-1}=0$ for $\cos(2\alpha)$. Fig. S1 in Supplementary Information shows an example of how these limits may be determined. Tables S2 to S4 give the integration limits for the static case and Tables S5 to S7 give those for the MAS case. In both cases, there are two regions that must be treated separately for the first integrand (Tables S2 and S5). For the second integrand, on the other hand, the integration regions depend upon whether η is less than or greater than the value at which an extra feature appears in the lineshape. This limiting value is 1/3 for the static case and 3/7 for the MAS case. Tables S3 and S6 contain the integration limits for the three ranges required for the second integrand below these values of η, whilst Tables S4 and S7 contain the integration limits for the four ranges required for the second integrand above these values of η. With the integration limits defined for any given value of f_Q, numerical integrations can be carried out to determine the lineshape. We have implemented these calculations in Mathematica 10.2 [27].

Fig. 1 shows an example of a calculated lineshape for a static second-order quadrupolar central transition with η=0.7. The full lineshape is shown, together with the contributions from the two integrands, $P_1(f_Q^{(Static)},\ \cos(2\alpha_{PL}))$ and $P_2(f_Q^{(Static)},\ \cos(2\alpha_{PL}))$. The singularities and steps due to the turning points in $f_Q^{(Static)}$ are also indicated. The regions with distinct integration limits lie between these turning points, specifically two regions for $P_1(f_Q^{(Static)},\ \cos(2\alpha_{PL}))$ and four regions for $P_2(f_Q^{(Static)},\ \cos(2\alpha_{PL}))$. Fig. 2 shows a similar view for the MAS case with η=0.8. Again, the contributions from the two

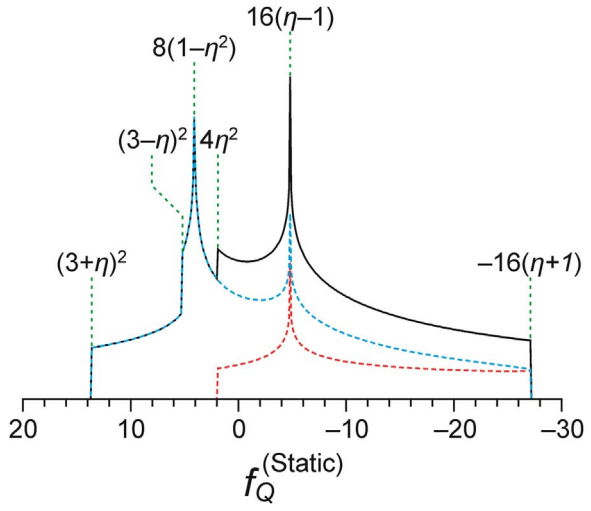

Fig. 1. Second-order quadrupolar central-transition lineshape for the static case with η=0.7. The total lineshape is shown in black, the contribution from the integrand $P_1(f_Q^{(Static)},\ \cos(2\alpha_{PL}))$ is shown in red and the contribution from the integrand $P_2(f_Q^{(Static)},\ \cos(2\alpha_{PL}))$ is shown in blue. The positions of the six singularities are indicated by the green lines. The horizontal scale corresponds to frequency in units of A_Q (Eq. (10)).

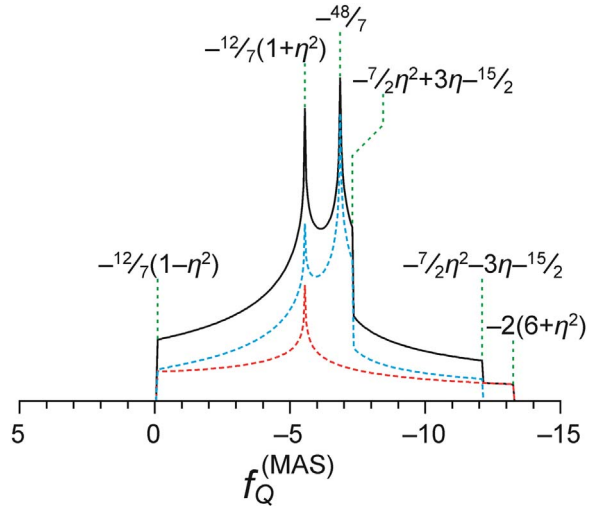

Fig. 2. Second-order quadrupolar central-transition lineshape for the MAS case with η=0.8. The total lineshape is shown in black, the contribution from the integrand $P_1(f_Q^{(MAS)},\ \cos(2\alpha_{PR}))$ is shown in red and the contribution from the integrand $P_2(f_Q^{(MAS)},\ \cos(2\alpha_{PR}))$ is shown in blue. The positions of the six singularities are indicated by the green lines. The horizontal scale corresponds to frequency in units of A_Q (Eq. (10)).

integrands, $P_1(f_Q^{(MAS)},\ \cos(2\alpha_{PR}))$ and $P_2(f_Q^{(MAS)},\ \cos(2\alpha_{PR}))$, are shown separately, together with the singularities and steps. We note that the two integrands correspond to distinct regions within the orientational distribution. Specifically, $P_1(f_Q^{(Static)},\ \cos(2\alpha_{PL}))$ and $P_1(f_Q^{(MAS)},\ \cos(2\alpha_{PR}))$ correspond to the "polar" regions (around β=0 and π) whereas $P_2(f_Q^{(Static)},\ \cos(2\alpha_{PL}))$ and $P_2(f_Q^{(MAS)},\ \cos(2\alpha_{PR}))$ correspond to the "equatorial" regions (around β=½π). We stress that no line broadening has been applied in either calculation.

In order to calculate the static lineshape with η=0.7, Field and Bain [10] used (Fig. 2 in their paper) a set of ~3.3×10^{10} Euler angle pairs (the 52nd Fibonacci number) generated by the ZCW algorithm [14–16], with the calculation taking *ca.* 15 h of processing time on a standard personal computer. In contrast, our calculation (Fig. 1 in the present paper) of the same lineshape with 408 points covering the non-zero portion of the spectrum (a resolution of 0.1 in $f_Q^{(Static)}$) took less than 9 s on a standard 3.0 GHz dual core PC running Mathematica 10.2 under Windows 7. We get very similar results for the MAS case. Again, only a few seconds are required to calculate the lineshape shown in Fig. 2, with a resolution of 0.05 in $f_Q^{(MAS)}$.

To ascertain the accuracy of the lineshape intensities, we can compare the theoretical values for the step heights and the centre of gravity [10]. For the step heights, we calculated the difference in intensity of two points on either side of the step, then reduced the frequency difference between those two points until the numerical integration became unstable due to the proximity of the step to the points. Table S8 contains the formulae for the absolute heights of the steps for the static case, considering a lineshape with unit integral. Based on the table in reference [10], Table S8 includes an analytical form for the step at $4\eta^2$. All step intensities for the static case with η=0.7 were found to be within 0.006% of the theoretical values. Furthermore, the difficulties encountered by Field and Bain in calculating the step intensity at $4\eta^2$ around the value of η=0.8 are eliminated and the value calculated by our method is within 0.0006% of the theoretical value. Our calculations of the step intensities for the MAS case also lie very close to the theoretical values [11] given in Table S9, which includes an analytical form for the step height at $-2(6+\eta^2)$ and a corrected version of the step height at $-(12/7)(1-\eta)^2$. Plots showing our calculated values for the step heights against the theoretical values are given in Supplementary Information (Figs. S2 and S3).

As a second verification of the accuracy of our lineshapes, we calculate the centre of gravity. For both the static and MAS cases,

integrating the function f_Q over all orientations gives the formula for the centre of gravity of the lineshape, which is at $f_Q = -(8/5)(3+\eta^2)$. Calculating the centre of gravity from the spectra in Figs. 1 and 2 gives values in excellent agreement with this theoretical value, illustrating that the lineshape is accurately calculated between the singularities. Indeed, across the full range of values of η, the centre of gravity is found to be well-predicted by our calculations, except in cases for which one or more of the calculated values of f_Q coincide with singularities, as these positions give rise to errors in calculating the centre of gravity.

4. A fully numerical method

In Section 3, we resorted to numerical integration at the last step when the function in Eq. (19) could not be integrated analytically. We now turn to cases for which, following the methodology of Pake, Bloembergen and Rowland, the *first* step cannot be carried out analytically. An example of such a lineshape arises for the combination of a static second-order quadrupolar interaction and a chemical shift anisotropy when the principal axis systems do not share the same alignment. In this case, the resonance frequency cannot be given in terms of powers of $\cos^2(\beta)$ alone (as in Eq. (14)). Instead, terms in $\sin(\beta)\cos(\beta)$ are also present. Consequently, the solutions for β as a function of f and α are far more complicated and cannot be easily handled by the semi-analytical method. What can we do under these circumstances, other than calculate the resonance frequency over a large number of evenly-distributed Euler angle pairs to arrive at an estimate of the lineshape? The answer is to follow the procedure described above, but in a purely numerical fashion.

To achieve this aim, we first recognize that the functions for β in terms of f and α correspond to contour lines (or sections of contour lines) on a plot of the resonance frequency against the Euler angles α and β. We can therefore consider the integration over α in Eq. (7) as equivalent to carrying out integration of the function along a contour line at the level f. If a usable equation for these contour lines cannot be derived, we can still carry out the integration numerically if we can define a set of points on each contour line and perform a sum, corresponding to the integration in Eq. (7), over these points. The required sum is

$$P(f) = \frac{1}{4\pi} \sum_{f(\alpha,\beta)=f} \sin(\beta) \left| \frac{\Delta\beta}{\Delta f} \right| \Delta\alpha, \tag{26}$$

where $\Delta\alpha$ is the increment in α between the points and $\Delta\beta/\Delta f$ is the reciprocal of the gradient of f parallel to the β axis. If the function for the resonance frequency can be differentiated with respect to β, this gradient can be calculated directly for each point, otherwise it can be determined by considering the gradient between two points on either side of the contour line at $\{\alpha, \beta + \tfrac{1}{2}\Delta\beta\}$ and $\{\alpha, \beta - \tfrac{1}{2}\Delta\beta\}$. Applying this summation gives good quality lineshapes in most cases but has a tendency for error at points on the contours parallel to the β axis since, at such points, both the gradient and $\Delta\alpha$ can be very small and their quotient is therefore more highly error prone. To avoid this problem, we note that the summation can also be performed as follows

$$P(f) = \frac{1}{4\pi} \sum_{f(\alpha,\beta)=f} \sin(\beta) \left| \frac{\Delta\alpha}{\Delta f} \right| \Delta\beta, \tag{27}$$

where $\Delta\alpha$ and $\Delta\beta$ have been exchanged. In fact, for any given pair of Euler angles, either the term in Eq. (26) or the term in Eq. (27) may be used in the sum. In practice, for each point on a contour line, we use the term that involves the larger gradient, thereby avoiding the problem associated with small values.

Implementing this fully numerical method proves to be rather challenging due to the difficulty of finding the points on each contour line. A program like Mathematica can produce a contour plot from which the points on the contour lines can be extracted. However, as these plots are produced by an interpolation method starting from a simple grid, the positions of the points on the contour lines are neither very accurate nor very evenly spaced along the contour lines. We have sought to overcome these difficulties by producing sets of points on each contour line using the following procedure.

1. All the maxima and minima for the function of the resonance frequency are identified by considering a finely-spaced grid of points, identifying the maxima and minima within this grid, then using these points as a starting position for a numerical minimization or maximization of the function.
2. Lines are constructed out of each minimum and maximum which allows at least one point to be found on every contour line for each value of the resonance frequency.
3. We then move around each contour line, identifying a set of points which are evenly spaced on the surface of the sphere, typically choosing a spacing of 0.01 rad. To avoid duplication, the first point of each new contour line is checked against those already calculated at the same level, taking into account the inversion symmetry that is always present for such functions [20].
4. We input these points into Eqs. (26) or (27) to give the contribution to the intensity of each point on the contour line for each resonance frequency.

Although this method is not fast, it does produce sets of points precisely on the contour lines. As each set of contour lines at a given level can be treated separately, this calculation should be amenable to parallelization, although we have not implemented a parallel version at this stage. When applied to interactions for which the lineshape can be calculated either analytically or semi-analytically, the lineshapes obtained using the numerical method, although slower to obtain, are very similar.

This fully numerical method is particularly advantageous for lineshapes that result from the convolution of more than one interaction, particularly when the two interactions do not share the same principal axis system. Fig. 3 shows a contour plot of the resonance frequency for a combination of a second-order quadrupolar interaction and a non-aligned chemical shift anisotropy (CSA) under static conditions. The function for this lineshape, denoted $f_{Q,C}^{(Static)}$, is defined through

$$\omega_{CT} = \omega_0\delta_{iso} + A_Q f_{Q,C}^{Static}, \tag{28}$$

and is given by

$$f_{Q,C}^{(Static)} = f_Q^{(Static)} + \frac{1}{A_Q} \sum_{n=-2}^{2} \sum_{m=-2}^{2} A_C^{(m)} D_{m,n}^2(\Omega_{CQ}) D_{n,0}^2(\Omega_{QL}). \tag{29}$$

We now denote the asymmetry parameter for the quadrupolar interaction as η_Q and that for the CSA as η_C. The terms in the sum for the CSA are given by $A_C^{(0)} = \delta_{aniso}$, $A_C^{(1)} = A_C^{(-1)} = 0$ and

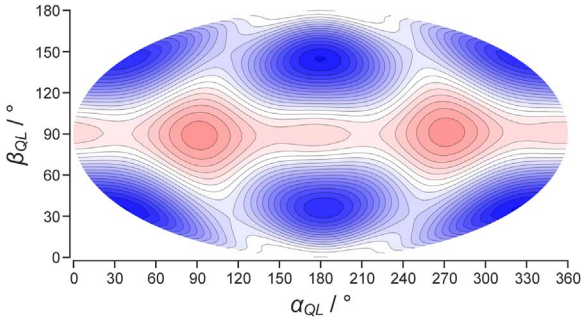

Fig. 3. Contour plot (employing a Mollweide-type projection [28]) of the resonance frequency $f_{Q,C}^{(Static)}$ with parameters η_Q=0.7, ω_0 δ_{aniso}=2A_Q, η_C=0.2, α_{CQ}=20°, β_{CQ}=50° and γ_{CQ}=35°. Shades of red indicate positive values, shades of blue indicate negative values. The α_{QL} scale refers to the values at β_{QL}=90°.

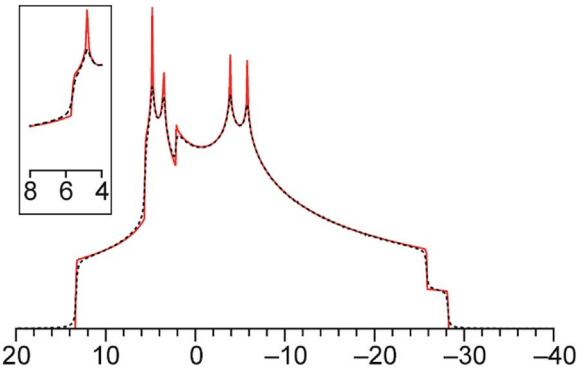

Fig. 4. Static central-transition lineshape for the combination of a second-order quadrupolar interaction and a chemical shift anisotropy with the same parameters as in Fig. 3 calculated using our fully numerical method (solid red line) and by a set of Euler angle pairs determined using the ZCW algorithm (dashed black line). The horizontal scale corresponds to frequency in units of A_Q (Eq. (10)). The inset shows the step at $f_{Q,C}^{(Static)} = 5.6$.

$A_C^{(2)} = A_C^{(-2)} = -(1/\sqrt{6})\eta_C\delta_{aniso}$. The Euler angles Ω_{CQ} relate the PAS for the CSA to that for the quadrupolar interaction. The values of the parameters are given in the caption of Fig. 3. In the contour plot, two distinct minima, three distinct maxima and four distinct saddle points can be seen. Consequently, the lineshape consists of five steps and four singularities.

Fig. 4 shows the lineshape for the centre band of this combined second-order quadrupolar interaction and non-aligned CSA. The lineshape consists of 416 points (at a resolution of 0.1 in $f_{Q,C}^{(Static)}$), calculated with Mathematica 10.2 in approximately 7 min, using a total of 210 897 pairs of Euler angles distributed evenly around the contour lines with a spacing between points of approximately 0.01 rad. No line broadening was applied. For comparison, the same lineshape was calculated (again using Mathematica 10.2) with the same frequency resolution in approximately 90 s by summing over a set of 196 418 (the 27th Fibonacci number) pairs of Euler angles distributed over a hemisphere, generated using the ZCW algorithm [14–16]. A Lorentzian lineshape was applied, with a half width at half height equal to the frequency spacing (0.1 in $f_{Q,C}^{(Static)}$) between the calculated points. Reducing the applied line broadening led to a noticeably less smooth shape, indicating that this angle set requires a line broadening of such a magnitude to generate a smooth lineshape.

Clearly, the two lineshapes in Fig. 4 are in good agreement, particularly in the regions between the steps and singularities. Furthermore, the positions of the steps and singularities match well. However, while the line broadening in the shape calculated using the ZCW algorithm leads to significant curvature around the steps, our lineshape has sharp features. This difference is particularly significant around the step at $f_{Q,C}^{(Static)} = 5.6$ (see inset in Fig. 4), which is quite clear in our lineshape but much harder to discern in that calculated using the ZCW algorithm. Although not clearly evident from the figure, the lineshape calculated using the ZCW algorithm is also somewhat noisier between the steps and singularities than that calculated by our method. We can therefore state that, for a similar number of Euler angle pairs, our method has produced a significantly better-quality lineshape.

Although sharper, our lineshape took rather longer to calculate. However, it must be noted that Mathematica is not the best choice for large-scale numerical calculations. We have also developed a Fortran code which replicates the specific calculation of the lineshape in Fig. 4 and which runs on the same computer in approximately 10 s. A further improvement which could be applied (in addition to parallelization) is an optimization of the spacing of the points on the contour lines. In principle, this can be increased for contours of lower curvature, thereby reducing the total number of points considered and the time required.

5. Conclusions

We have presented two new methodologies for calculating solid-state NMR lineshapes. The first method, applied to the second-order quadrupolar central-transition lineshape under both static and MAS conditions, avoids the need for large Euler angle sets to obtain accurate simulations and allows these lineshapes to be calculated in a matter of seconds without sacrificing accuracy. We call this methodology "semi-analytical", as it employs analytical formulae for the integrands and limits in the final numerical integration.

This methodology could clearly be applied to the calculation of other lineshapes. The key step is finding an analytical form for one of the Euler angles defining the resonance frequency. If such an expression or expressions can be derived, the required integrand(s) can be determined in a straight-forward manner, leaving only the numerical integration to be performed. The two cases presented in this paper are both amenable to determining formulae for the limits of the numerical integrations but, if this is not possible or desirable, the limits could be determined "on the fly" by identifying the regions over which each integrand is real-valued for each value of the resonance frequency.

The second method calculates a set of Euler angles specific to the problem in hand in a relatively efficient manner by only considering points which contribute to specific frequencies within the lineshape. Although much slower than the "semi-analytical" method, the second method is more generally applicable, as demonstrated by our calculation of the lineshape for the case of a combination of two interactions for which the principal axis systems are not aligned. This work extends earlier studies of mutually-oriented interactions by Chu and Gerstein [29].

We hope that the new methodologies presented here may stimulate new approaches to the calculation of lineshapes which may further enhance the power of solid-state NMR to study materials that give complicated lineshapes. In particular, the ability to simulate lineshapes rapidly and accurately will allow significantly improved fitting procedures to be implemented for determining the parameters that give rise to these lineshapes. We also note that the problem of efficient averaging over a sphere is of great interest in the field of EPR, where similar lineshape calculations are required [30]. Thus, future applications in the EPR field are also anticipated.

Finally, we note that our methodologies cannot be applied to the simulation of certain types of NMR spectrum. We highlight two cases of this type, both of which will profit from further consideration. The first case concerns spectra for which both the frequency and linewidth are orientationally dependent, such as ^{2}H exchange spectra; although analytical expressions for both frequency and linewidth can be derived, the variable linewidth cannot be incorporated into our methodology in its current form. The second case concerns spectra for which an analytical expression for the frequency cannot be derived, requiring simulation to be carried out in the time domain, followed by Fourier transformation. In both cases, it remains imperative to identify sets of Euler angles which do not introduce distortions to the lineshapes.

Appendix A. Supplementary material

Supplementary data associated with this article can be found in the online version at http://dx.doi.org/10.1016/j.ssnmr.2016.10.002.

References

[1] G.E. Pake, J. Chem. Phys. 16 (1948) 327–336.
[2] N. Bloembergen, T.J. Rowland, Acta Met. 1 (1953) 731–746.
[3] A. Jerschow, Prog. Nucl. Magn. Reson. Spectrosc. 46 (2005) 63–78.
[4] K. Narita, J. Umeda, H. Kusumoto, J. Chem. Phys. 44 (1966) 2719–2723.
[5] D. Müller, Ann. Phys. 494 (1982) 451–460.
[6] A. Samoson, E. Lippmaa, A. Pines, Mol. Phys. 65 (1988) 1013–1018.
[7] K.T. Mueller, B.Q. Sun, G.C. Chingas, J.W. Zwanziger, T. Terao, A. Pines, J. Magn. Reson. 86 (1990) 470–487.

[8] L. Frydman, J.S. Harwood, J. Am. Chem. Soc. 117 (1995) 5367–5368.
[9] Z.H. Gan, J. Am. Chem. Soc. 122 (2000) 3242–3243.
[10] T.R. Field, A.D. Bain, Solid State Nucl. Magn. Reson. 61- 62 (2014) 39–48.
[11] T.R. Field, A.D. Bain, Solid State Nucl. Magn. Reson. 63- 64 (2014) 42–47.
[12] D.L. VanderHart, H.S. Gutowsky, T.C. Farrar, J. Am. Chem. Soc. 89 (1967) 5056–5057.
[13] A. Ponti, J. Magn. Reson. 138 (1999) 288–297.
[14] S.K. Zaremba, Ann. Mat. Pura Appl 73 (1966) 293–317.
[15] H. Conroy, J. Chem. Phys. 47 (1967) 5307–5318.
[16] V.B. Cheng, H.H. Suzukawa, M. Wolfsberg, J. Chem. Phys. 59 (1973) 3992–3999.
[17] D.W. Alderman, M.S. Solum, D.M. Grant, J. Chem. Phys. 84 (1986) 3717–3725.
[18] D. Wang, G.R. Hanson, J. Magn. Reson. 117 (1995) 1–8.
[19] M. Bak, N.C. Nielsen, J. Magn. Reson. 125 (1997) 132–139.
[20] M. Edén, M.H. Levitt, J. Magn. Reson. 132 (1998) 220–239.
[21] M.J. Mombourquette, J.A. Weil, J. Magn. Reson. 99 (1999) 37–44.
[22] G. Ajoy, J. Ramakrishna, S. Bahçeli, J. Klinowski, Solid State Nucl. Magn. Reson. 16 (2000) 305–338.
[23] R.E. Wasylishen, S.E. Ashbrook, S. Wimperis, NMR of Quadrupolar Nuclei in Solid Materials, Wiley, Chichester, 2012.
[24] A. Abragam, Principles of Nuclear Magnetism, Oxford University Press, Oxford, 1961.
[25] M.H. Cohen, F. Reif, Solid State Phys. - Adv. Res. Appl. 5 (1957) 321–438.
[26] E. Kundla, A. Samoson, E. Lippmaa, Chem. Phys. Lett. 83 (1981) 229–232.
[27] Wolfram Research, Inc., *Mathematica 10.2*; Champaign, Illinois, 2015
[28] K.B. Mollweide, Mon. Corr. Beförd. Erd.- Himmels-Kunde 12 (1805) 152–163.
[29] P.J. Chu, B.C. Berstein, J. Chem. Phys. 91 (1989) 2081–2101.
[30] C. Crăciun, J. Magn. Reson. 245 (2014) 63–78.